

Origin and morphology of barchan and linear clay dunes in the Shuhongtu Basin, Alashan Plateau, China

Fangen Hu^{a,*}, Xiaoping Yang^b, Hongwei Li^{b,*}

^a Yichun University, Yichun 336000, China

^b Department of Earth Sciences, Zhejiang University, Hangzhou 310027, China

ARTICLE INFO

Article history:

Received 6 January 2019

Received in revised form 6 April 2019

Accepted 14 April 2019

Available online 29 April 2019

Keywords:

Clay dunes

Alashan Plateau

Migration rates

Sediment source

Grain-size

ABSTRACT

Clay dunes are characterized by a relatively high content of silt and clay and are typically developed on the lee side margin of closed-basins in arid and semi-arid areas. Although they are widely distributed aeolian landforms on Earth, little is known about their development and distribution in Asia. Our field investigations have identified for the first time the occurrence of clay dunes in the Alashan Plateau, north China. The clay dunes occur in three isolated lowland areas of the Shuhongtu (SHT) Basin and their morphologies (barchans, hooked barchans, asymmetrical barchans, and linear or seif dunes) differ substantially from those of the well-studied clay dunes in Australia, Africa and North America. These differences could be mainly attributed to the asymmetrical bimodal wind regime, prolonged drought and sediment physical properties, which indicate that dunes of any type can be formed in sand, silt or clay. Based on the known evolution of the SHT paleo-lake basin and regional climate change, we infer that the landscape of modern clay dunes in the desert of the Alashan Plateau does not predate MIS 5, and probably formed during the late Holocene. Analyses of grain-size distributions and the contents of trace and rare earth elements, combined with geomorphological characteristics, indicate that the source sediments of the clay dunes are mainly local Cretaceous-Tertiary and Quaternary red fluvial-lacustrine mudstone and sediments, while the ultimate source is the weathered and denuded products of granitoids of the East Altay Mountains. Comparison of the morphology and alignment of the clay dunes with the prevailing wind pattern tends to support Tsao's (1984) model of the transition in dune shape from barchans to seif or linear dunes. During 2003–2013, the seif or linear dunes of the SHT Basin migrated laterally and elongated northeastward at rates of about 2–4 m/yr and 16–20 m/yr, respectively.

© 2019 Elsevier B.V. All rights reserved.

1. Introduction

Aeolian dunes on the Earth's surface are major landforms and unique geomorphological and palaeoclimatic indicators in arid and semiarid zone (Thomas and Burrough, 2012). Their state is defined by sediment supply, sediment availability and the transport capacity of the wind (Kocurek and Lancaster, 1999). Climatic signals are preserved in a dune's morphology and stratigraphy, and dunes have been shown to be a valuable paleoenvironmental archive in arid and semi-arid areas (Lancaster et al., 2002; Thomas and Burrough, 2012; Yang et al., 2013, 2015; Williams, 2014). On Earth, dune sediments consist mainly of fine- to medium-grained quartz, derived from fluvial, alluvial, coastal, or lacustrine systems (Yang, 1991; Lancaster, 1995; Pye and Tsao, 2008; Szykiewicz et al., 2010). Less common are sources bordering aeolian dunes that are composed of clays and silts derived from the deflation of neighboring pans or playas (Thomas, 2011; Goudie and Wells, 1995; Bowler, 1973). Such dunes are known as clay dunes (Huffman

and Price, 1949), termed lunette dunes in Australia (Edwin and Hills, 1940; Chen, 1995) and dubbed clay-lunette dunes in some references (Bowler, 1973; Dare-Edwards, 1984; Thomas, 2011), but not all lunettes are formed from clay (Hesp and Smyth, 2019). In general, the term 'clay dunes' as opposed to 'dunes-with-clay' refers to dunes with a clay content exceeding ~15%, because a clay content exceeding 15% is usually sufficient to render a dune's morphological and structural characteristics distinct from those of well-sorted sand dunes (Bowler, 1973). By reason of their relatively rare occurrence, however, clay dunes have attracted much less attention than sand dunes.

Clay dunes were first described by Coffey (1909) from field investigations in Texas. In contrast to sand dunes, their distinguishing feature lies in the occurrence of substantial amounts of clay which exert a controlling influence on their formation, evolution, morphology and structure (i.e. bedding characteristics and dip angle) (Bowler, 1973; Holliday, 1997; Telfer and Thomas, 2006; Rubin and Hesp, 2009). Clay dunes have been studied in North America (Price, 1963; Holliday, 1997; Holliday et al., 2008; Rich, 2013; Munroe et al., 2017), Argentina (Dangavs, 1979), Australia (Edwin and Hills, 1940; Bowler, 1973, 1983), Southern Africa (Lancaster, 1978; Thomas et al., 1993; Marker and Holmes, 1995),

* Corresponding authors.

E-mail addresses: hufg1112@jxycu.edu.cn (F. Hu), lihw@zju.edu.cn (H. Li).

Nigeria and Tunisia (Bowler, 1973; Goudie and Wells, 1995), and Europe (Bernat Rebollal and Pérez-González, 2008), almost covering all the continents of the Earth. However, there are few studies of clay dunes in Asia as to date.

Previous studies have demonstrated that clay dunes are important paleoenvironmental archives attesting to changing climatic and hydrological conditions and associated geomorphic processes of lake-dune systems (Lees and Cook, 1991; Chen, 1995; Sabin and Holliday, 1995; Marker and Holmes, 1995; Lawson and Thomas, 2002; Telfer and Thomas, 2006; Fitzsimmons et al., 2007; Bowen and Johnson, 2012; Rich, 2013). For example, on the Southern High Plains of the U.S.A., clay dune construction corresponded with episodes of greater aridity at ~277–233 ka, ~206–154 ka, ~131–92 ka, ~16–11 ka, ~7–5 ka, and post-5 ka, when a dry climate promoted basin desiccation and aeolian processes acted to excavate, deflate and deepen lake/playa basins (Holliday, 1997; Rich, 2013). The deflation increased the potential for the accumulation of clay in deeper water during less windy periods, and the deposition of sand-sized aggregates of clay on the lee-side resulted in the formation of clay dunes (Holliday, 1997; Rich, 2013).

Clay dunes usually occur along the downwind margins of shallow saline lake basins in arid and semi-arid regions, such as pan, playa and ephemeral lakes in closed basins (Sabin and Holliday, 1995; Goudie and Wells, 1995; Lancaster, 1986). However, the formation mechanism of clay dunes is still controversial. Some studies argue that clay dunes were constructed during hydrologically positive basin stages by deflation from wave-accumulated beach sediments on the downwind margins of playas (Killigrew and Gilkes, 1974; Lees and Cook, 1991). The most useful conceptual framework concerning clay dune development remains that they are built from the accumulation of sand-sized aggregates of clay pellets under the condition of lake-level falling (Bowler, 1973, 1986; Lancaster, 1978; Price, 1963; Holliday, 1997). The resultant pellets, formed by the efflorescence of salts or by the mechanical disintegration of mud curls, were trapped by salt-tolerant plants growing around the margins of the playas to form clay dunes (Bowler, 1973; Price, 1963; Hesp and Smyth, 2019).

Many intermontane basins, playas and ephemeral lakes in the mid-latitude desert belt of Asia, such as Lop Nor, Qarhan and Chaka Lake in northwest China, have been recognized. In principle, although there should be an abundance of clay dunes in these areas, they have not been reported so far. In November 2013, our field investigations identified for the first time the occurrence of clay dunes in the Alashan Plateau of northwest China (Hu and Yang, 2016). Morphologically, most clay dunes are barchan, asymmetric barchan and seif dunes (sometimes be called linear dune, Lancaster, 1995). The meandering crest (sinuous ridge) is the essential feature of seif dunes, but detailed shape of which varies under different wind regime. Many seif dunes in northern Sinai are highly sinuous in plan, but some are relatively straight (Tsoar, 1978). Owing to different classification or names, linear dune is commonly referred to as a seif dune in North Africa and Saudi Arabia, as a sand ridge in Australia, and as a longitudinal dune in many other places (Pye and Tsoar, 2008). The morphologies of these dunes differ substantially from the above-mentioned clay dunes in North America and Australia (Coffey, 1909; Bowler, 1973; Sabin and Holliday, 1995), where the dunes are often crescentic in shape, but the horns point towards rather than away from the wind. We present the results of the first study of clay dunes in north China, and use geochemical and granulometric analyses, combined with satellite images, wind data and field observation, to systemically analyze the distribution, morphological evolution, and origin of the clay dunes in Alashan Plateau. Our overall aim was to advance our understanding of the formation of clay dunes.

2. Regional setting

The Alashan Plateau, located in north China, in the mid-latitude desert belt of Asia, is surrounded by the Mongolian Altay Mountains to the

north, the Beishan Mountains to the west and the Qilian Mountains to the south (Fig. 1). The terrain has been subjected to long-term continuous uplift and denudation (BGMIRM, 1991; Wu and He, 1993) and consists of fault-block mountains and several faults basins, such as Ejina Basin and Suhongtu (SHT) Basin, in west and north, respectively. The Alashan Plateau is characterized by low relief, with the elevation decreasing gradually from 1600 m in the south to 900 m in the north (Fig. 1). Due to the dry and windy climate, Gobi desert, sand dunes, yardangs and playas are the major landforms in the region. The Badain Jaran, Tengger and Wulanbuhe sand seas, and several small dune fields such as Yamalik, are distributed across the plateau and contribute large amounts of dust to the Chinese Loess Plateau and the western Pacific Ocean (Hu and Yang, 2016; Sun et al., 2008).

The clay dunes occur in the SHT Basin, a rift basin in the northeastern Alashan Plateau, located between the Yagan and Engerwusu fault belts (Wu and He, 1993) which were formed during the Cretaceous (Li and Zhou, 1997) (Figs. 1 and 2). The SHT Basin is bounded by the Shalazha Mountains to the south and the East Altay Mountains to the north (Fig. 2a). Geologically, the SHT Basin and Ejina basin are sub-basins of the larger Ejina-Yingen Basin, and previously a broad river valley (presently buried by sand dunes of the Badain Jaran Desert) connected the two sub-basins and forming a unified drainage system during the Quaternary (Guo et al., 2000). On the edge of the SHT Basin, basement rocks are mainly Paleozoic granitoid and gabbro, and they are overlain by Cretaceous-Tertiary lacustrine sandstone and mudstone, conglomerates and basalt (Li and Zhou, 1997). Surface sediments are mainly Quaternary fluvial-lacustrine deposits and aeolian sand (Li and Zhou, 1997; Guo et al., 2000; Shi et al., 2014). In addition to the clay dunes, sand dunes are also developed on the outer fringes of the SHT Basin, primarily in the northern piedmont of the Shalazha Mountains; most of them are nebkhas, oblique dunes, transverse dunes and barchanoid ridges with NNE-SSW or NE-SW alignments. The study area now has a cold-desert climate, with mean annual temperature and precipitation (data obtained online from the U.S. National Climatic Data Center, <http://www.ncdc.noaa.gov/cdo-web/datasets>) of 7.9 °C and 102 mm, respectively. The wind strength and direction are mainly controlled by the East Asian Monsoon system, which results in pattern of alternating southeast winds in summer and northwest winds in winter. Monthly wind records (data obtained online from the U.S. National Climatic Data Center, <http://www.ncdc.noaa.gov/cdo-web/datasets>) from the nearest meteorological station (Bayan Mod, 40.75°N, 104.5°E, ~75 km from the study area) spanning 1983–2012 show that the dominant sand-transporting winds in the area are from the northwest (Fig. 1), driven by the winter monsoon which blows from the Siberian High Pressure system. Nevertheless, due to the impact of topography, the sand rose for the station of Hails (41.45°N, 106.383°E, ~130 km from the study area, in the east of the SHT Basin), exhibits a multimodal wind regime (Fig. 1).

3. Materials and methods

During field investigations, three clay dunes fields were identified in the SHT Basin, Alashan Plateau. In order to shed light on their origin and evolutionary processes, we investigated the clay dunes distribution, morphological and geomorphological characteristics, such as areas, dune types, lengths, width and surface characteristics of clay dunes. In the meanwhile, some samples of clay dunes were collected in the A1 area (Fig. 2a, b) for grain size and geochemistry analyses. Samples 1 and 2 are located on the outer edge of the clay dune field and were collected from active and fixed sand dunes, respectively. Samples 3–7 and 9 were collected from the crest of the clay dunes, while samples 4 and 6 were collected from coarser sand on the rippled surface of the dune crest, which has a higher sand content. Sample 8 was collected from the inter-dune area and represents basin floor (paleo-lake floor) sediments. In addition, in order to trace the sediment source of the clay dunes, two fluvial-lacustrine silty clay samples (marked by FLS1 and FLS2) were also collected from outcrops for comparison. Sample FLS1

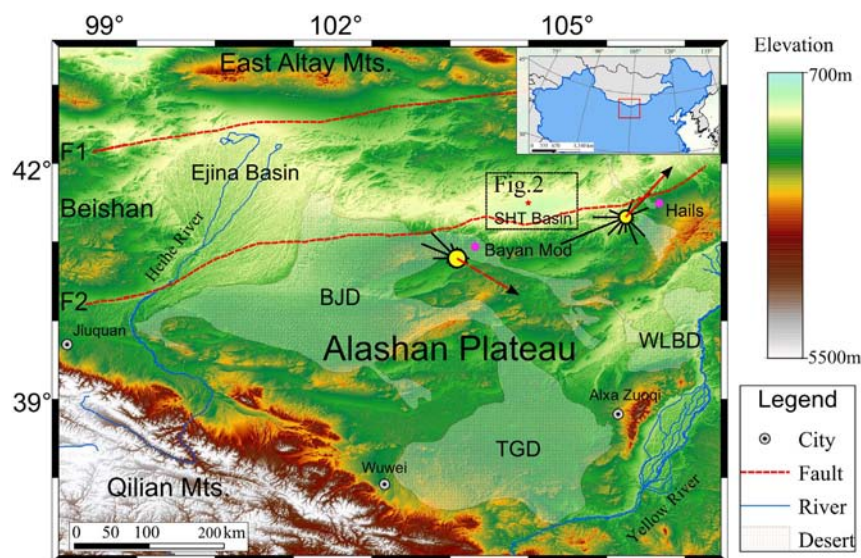


Fig. 1. Topographic map (derived hillshade DEM, data from STRM, <http://www.gscloud.cn>) showing the Alashan Plateau in north China, and deserts distributed within the plateau. Also shown are sand roses for the two nearest meteorological stations to the SHT Basin; black lines show sand drift potential (DP) and red arrows indicate the resultant sand drift potential (RDP). The red star represents the sampling location in Fig. 2. BJD: Badain Jaran Desert; TGD: Tengger Desert; WLBD: Wulanbuhe Desert; SHTB: Suhongtu Basin; F1: Yagan fault belt; F2: Engerwusu fault belt.

is from weathered mudstone overlying Cretaceous volcanic rocks, and sample FLS2 is the well-known Tertiary red clay exposed by wind erosion (BGMRI, 1991).

Grain-size distributions of the samples were measured using a Coulter LS13 320 laser grain-size analyzer, with a measurement range of 0.375–2000 μm , in the Key Laboratory of Cenozoic Geology and Environment, Institute of Geology and Geophysics, Chinese Academy of

Sciences. About 0.5–1 g of sediment from each air-dried, disaggregated sample was pretreated with 10 ml of 30% H_2O_2 to remove organic matter, and then with 10 ml of 10% HCl to remove carbonates. The organic- and carbonate-free samples were diluted and rinsed to neutral pH followed by centrifugation. Finally, 10 ml of 10% $(\text{NaPO}_3)_6$ was added for dispersion prior to grain-size analysis. In order to show that the clay component of the samples was transported in the form of sand-

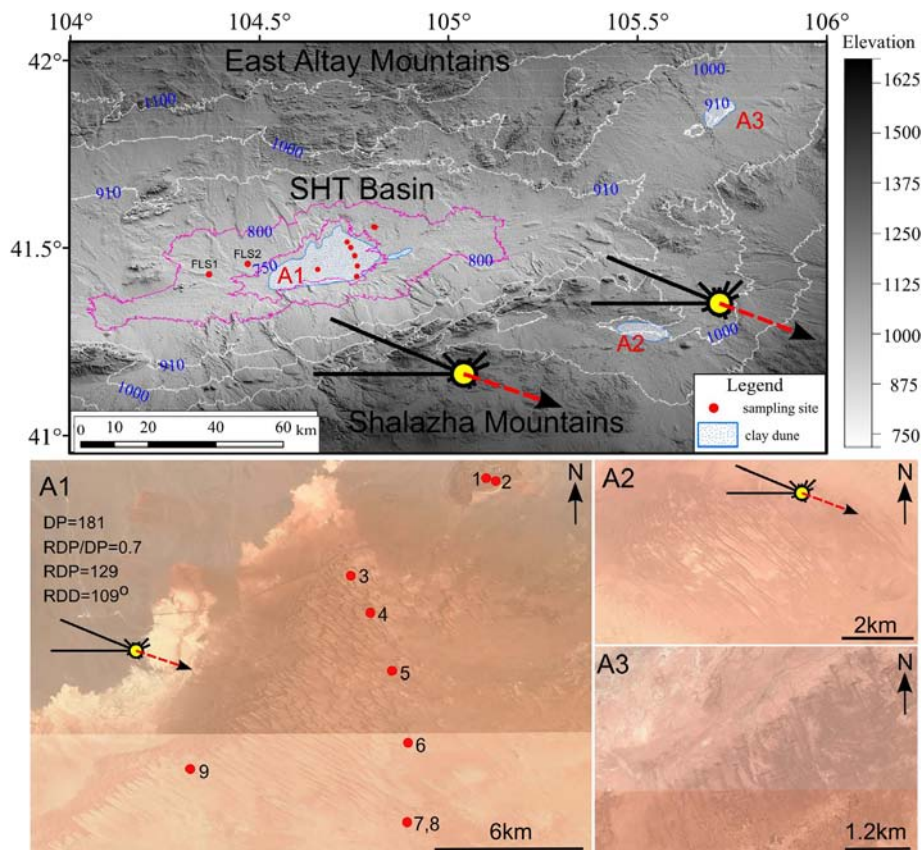


Fig. 2. Upper: Location of the study area and contour line delimiting the SHT Basin (data from ASTER GDEM, <http://www.gscloud.cn>), and sand roses with the same format as in Fig. 1. Lower: clay dunes distributed in SHT Basin and location of sampling sites (modified from a Google Earth image and source data from GeoEye-1 Satellite Sensor).

sized aggregates, dry sieving method was also conducted on samples 5 and 7 using an AS200 Sieving Shaker for 30 min at 0.25 ϕ intervals. Grain-size- related statistical parameters were calculated according to Folk and Ward (1957), using the program Gradistat (<http://www.kpal.co.uk/gradistat.html>) developed by Blott and Pye (2001).

Given that clay dunes are mainly composed of clay and silt, geochemical analysis was conducted on bulk samples and the fine fraction (clay and silt) that was extracted by dry sieving of the bulk samples. The geochemical data from samples 1–9 are from Hu and Yang (2016), and those from samples FLS1 and FLS2 are presented here for the first time. Trace and rare earth elements were determined using an ICP-MS in the Beijing Research Institute of Uranium Geology, Chinese Ministry for Nuclear Industries. Rh was used as the internal standard. The samples were digested in a mixture of HNO_3 (1,1) and HF under high temperature and pressure, following the four-step procedure described in Yang et al. (2007). The analytical uncertainties (relative standard deviation) are less than $\pm 5\%$ and less than $\pm 1\%$ for rare earth elements (REE) determinations.

Historical Google Earth images were used to determine the migration rates of different dune forms (barchans, asymmetrical barchans and linear dunes). With a ground spatial resolution of ~ 0.4 m, the images were acquired on 12 July 2003, 16 June 2010 and 15 May 2013, respectively. A road, fluvial channels and bedrock outcrops were used as fiducial markers to co-reference the images. The dune crest locations were then mapped from the historical images to determine migration rates.

Wind records (data obtained online from the U.S. National Climatic Data Center, <http://www.ncdc.noaa.gov/cdo-web/datasets>) covering the period from 1983 to 2012 from the two nearest meteorological stations (Bayan Mod and Hails), on the periphery of the study area, were used to interpret potential sand movement and dune morphology (Fig. 1). However, considering the impact of topography on the wind regime (the Shalazha Mountains to the south, and the East Altai Mountains to the north) and the large distances involved (Fig. 2), European re-analysis (ERA) -Interim reanalysis wind data (<http://apps.ecmwf.int/datasets/>) from sites around the SHT Basin were also used to interpret potential sediment movement. The reanalysis near-surface wind data ranging from 1983 to 2012 with a horizontal spatial resolution of $0.75^\circ \times 0.75^\circ$ (a horizontal resolution of 79 km) and a time resolution of 6 h are processed to generate wind power parameters (Fig. 2b, only two data are available at the SHT Basin): Drift Potential (DP, numerically

expressed in vector units), Resultant Drift Direction (RDD), Resultant Drift Potential (RDP), and the ratios of RDP/DP which give a measure of variability in wind direction (Fryberger and Dean, 1979).

4. Results

4.1. Distribution and morphology of clay dunes in the SHT Basin

An analysis of the distribution and morphology of clay dunes can shed light on their origin and evolutionary processes. As shown in Fig. 2a, the clay dunes are restricted to the SHT Basin, and are mainly concentrated in the areas of A1, A2 and A3. Area A1, located in the center of the depression, has an elevation of ~ 740 m and covers an area of ~ 254 km². Areas A2 and A3, located in the northeastern and southeastern edges of the SHT Basin, have elevations of < 910 m and < 1000 m, respectively, and occupy an area of ~ 30 km². In terms of morphology, various types of clay dune co-exist in the SHT Basin. According to the classification system of McKee (1979), most of the clay dunes in area A1 are linear or seif dunes (Fig. 3a, b) with a NW orientation and approximately equal spacing (Fig. 3a), indicating a bidirectional wind regime. In addition, many barchan dunes and nebkhas occur in the northwestern and south-southeastern margin of area A1 (Fig. 3e, f), while small numbers of barchanoid ridges occur in the northwest part of area A2 (Fig. 2c); both types indicate unidirectional wind regimes. In addition, in area A3, there are also hooked barchans, a transitional form between barchans and linear dunes. In general, most of the linear clay dunes have lengths ranging from hundreds to thousands of meters, with the longest dunes reaching ~ 3.4 km and 3.6 km in areas A1 and A2, respectively. The height of all types of clay dune are relatively low, ranging from about 2–5 m, while the width of most of the linear dunes ranges from about 20–40 m. The clay dunes in the SHT Basin commonly have a gentle windward face and steeper slip face, similar to the sand dunes, whereas the smooth crest and shallow gullies on the stoss face (Fig. 3c, d) differentiate them from sand dunes.

4.2. Grain-size characteristics

Grain-size frequency distributions and associated statistical parameters, such as unimodal and multimodal distributions, and sorting, can provide information on particle properties, potential sources and transport pathways (Lancaster et al., 2015). Grain-size distributions of clay

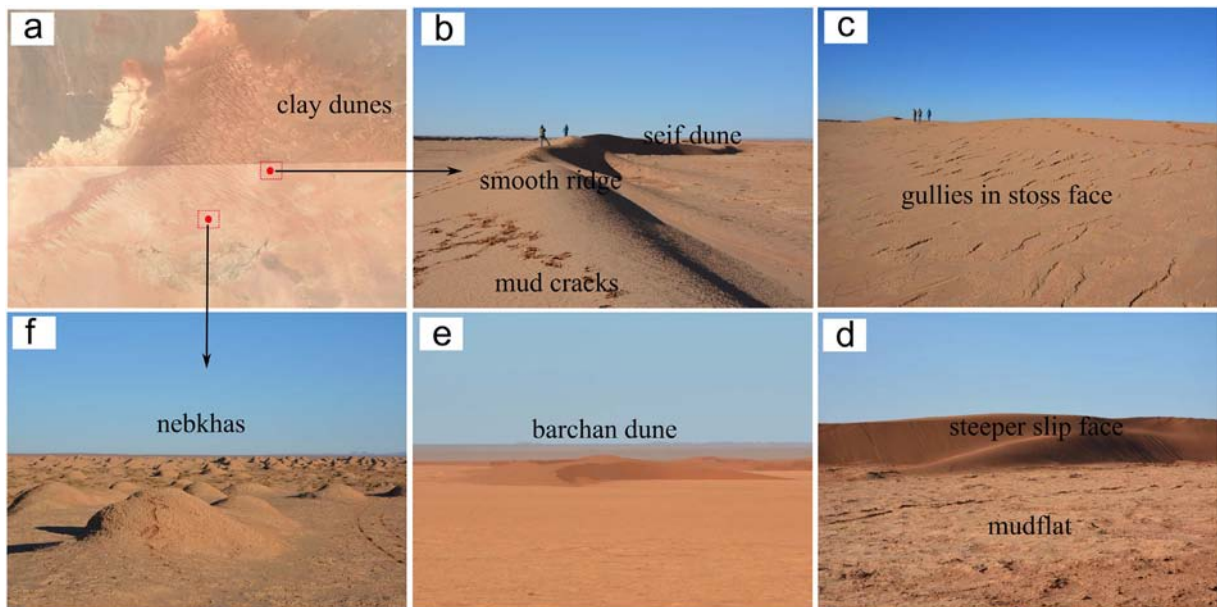


Fig. 3. Photographs showing the clay dunes in SHT Basin. Note the mud cracks on the surface of the clay dune and interdune, and the clay dune morphologies.

dune samples, and comparisons with those of fluvial sediments and aeolian dune sand, are presented in Fig. 4. The clay dune samples generally have bimodal or trimodal distributions, while samples 1 and 2 are unimodal distributions. In terms of distribution, all of the samples can be divided into three groups, as shown in Fig. 4a, b, and c. The first group (samples 3, 5 and 7–9) exhibits two peaks, both of equal magnitude, with ranges of 4–6 μm and 180–500 μm (Fig. 4a). For the second group (samples 4, 6), the main mode is at $\sim 700 \mu\text{m}$, while the second mode is around 4–6 μm , (Fig. 4b). The unimodal distribution of the third group (samples 1, 2) reflects a classical aeolian dune sand type, although sample 2 has a second peak at 4–5 μm (Fig. 4c). These results broadly agree with our field observations and analysis of grain-size cumulative frequency curves (Fig. 4d, e, f) and related parameters (Tables 1 and 2).

Notably, the grain-size distribution of clay dune samples (samples 5 and 7) determined by standard sieving has a unimodal distribution (with the mode at around 200–300 μm); the samples are well-sorted, have a sandy texture (98% >63 μm) and a medium diameter of 200 μm , similar to the characteristics of classical aeolian dune sand (Fig. 5). This suggests that the clay and silt are transported and accumulated as sand-sized aggregates.

Compared to the sand dune samples (samples 1 and 2), the particle size composition of clay dune samples (Table 1) are characterized by a higher content of silt and clay, within the range of 29.56–65.10% (the silt and clay content of sample 8, representing lake-floor sediments, is 71.3%). Samples 4 and 6 are mainly composed of coarse sand and silt, whereas other clay dune samples are dominated by silt and fine sand. The grain-size distribution of sample 1 has characteristics indicative of typical aeolian dune sand (Yang, 1991), consisting of fine to medium sand (84.52%). The samples range widely in their grain-size, from silt to medium sand (Table 2), but all are poorly to very-poorly sorted. Most of the clay dunes have a mean grain-size ranging from 5.02 to 6.12 ϕ (30.79–14.38 μm), and exhibit distributions which are highly platykurtic and coarse-skewed (with a fine tail). However, samples 4

Table 1

Grain size composition of sediment samples from the study area. The –S* suffix indicates determined by standard sieving.

Sample	<63 μm	63–125 μm	125–250 μm	250–500 μm	500–1000 μm	1000–2000 μm
1	5.85	4.06	25.91	54.55	9.63	0.00
2	26.00	46.77	27.22	0.02	0.00	0.00
3	61.90	2.70	9.10	15.80	10.50	0.00
4	29.56	1.78	4.28	7.56	42.96	13.86
5	65.10	9.40	18.00	6.60	0.90	0.00
6	34.80	3.10	9.10	13.80	36.40	2.80
7	50.50	9.60	22.90	16.30	0.70	0.00
8	71.30	7.00	20.30	1.40	0.00	0.00
9	59.30	3.20	11.60	23.80	2.10	0.00
5-S*	1.70	2.43	26.49	49.27	19.78	0.33
7-S*	0.00	0.25	36.48	54.83	8.32	0.12
FLS-2	100	0.00	0.00	0.00	0.00	0.00

and 6 are very fine skewed (with a coarse tail), with respective mean grain-sizes of 2.89 ϕ (135.2 μm), 3.37 ϕ (96.77 μm); thus, they are much coarser than the other clay dune samples. Samples 1 and 2 have distributions which are very fine-skewed and very leptokurtic, but with a large difference in their mean grain-size: 1.82 ϕ (283.1 μm) and 4.39 ϕ (47.84 μm), respectively.

4.3. Trace and rare earth elements

The Upper Continental Crust (UCC) normalized abundances of selected trace elements for the clay dune samples are illustrated in Fig. 6a, b. In general, compared to the UCC (Taylor and McLennan, 1985), the bulk samples are depleted in most of the trace elements which are enriched in the fine fraction (silt and clay); this is especially the case for the high field-strength elements (HFSE) Zr and Hf, which are almost 2 to 7 times higher than those of UCC. Among all the bulk samples (Fig. 6a), sample 8, which represents basin-floor sediments,

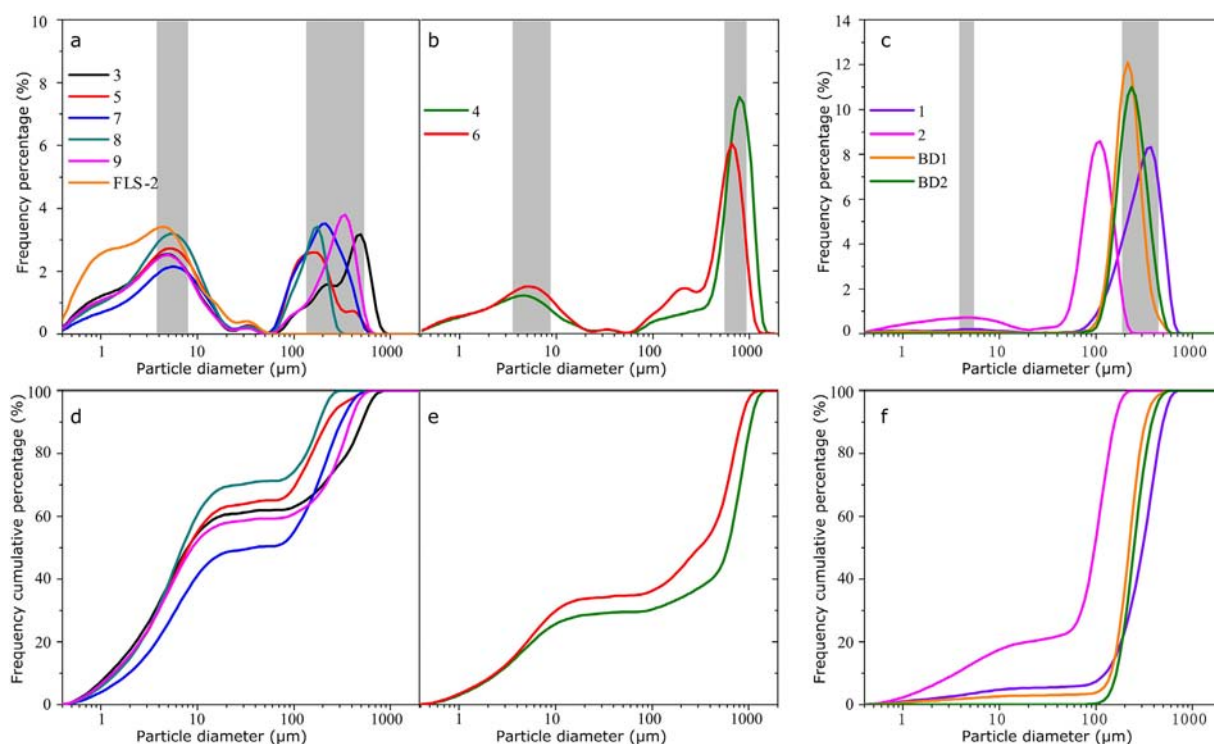


Fig. 4. Grain size-distributions and cumulative frequency curves of clay dune samples, with comparison to fluvial sediments and aeolian dune sand sediments. BJ represents samples collected from dunes crest in the Badain Jaran Desert. Samples 1 and 2 were collected from active and fixed sand dunes, respectively; samples 3–7, and 9 were collected from the crests of clay dunes; samples 4 and 6 were taken from the coarser sand on the rippled surface of the crest of clay dunes; and sample 8 represents the basin floor (paleo-lake floor) sediment. Samples FLS1 and FLS2 are from fluvial-lacustrine sediments collected from outcrops.

Table 2
Grain size statistic parameters for the studied sediment samples.

Sample	Distribution	Mean grain size (um)	Mean grain size (Phi)	Sorting (Phi)	Skewness (Phi)	Kurtosis (Phi)	Sorting skewness kurtosis		
1	Unimodal	283.1	1.82	1.19	0.47	2.24	Poorly sorted	Very fine skewed	Very leptokurtic
2	Bimodal	47.84	4.39	2.06	0.74	2.50	Very poorly sorted	Very fine skewed	Very leptokurtic
3	Trimodal	18.27	5.77	3.40	−0.39	0.60	Very poorly sorted	Very coarse skewed	Very platykurtic
4	Bimodal	135.2	2.89	3.43	0.82	0.61	Very poorly sorted	Very fine skewed	Very platykurtic
5	Trimodal	14.38	6.12	2.87	−0.32	0.65	Very poorly sorted	Very coarse skewed	Very platykurtic
6	Trimodal	96.77	3.37	3.33	0.66	0.59	Very poorly sorted	Very fine skewed	Very platykurtic
7	Bimodal	30.79	5.02	2.87	0.17	0.63	Very poorly sorted	Fine skewed	Very platykurtic
8	Bimodal	13.22	6.24	2.73	−0.35	0.64	Very poorly sorted	Very coarse skewed	Very platykurtic
9	Bimodal	18.11	5.79	3.20	−0.34	0.58	Very poorly sorted	Very coarse skewed	Very platykurtic
5-S*	Bimodal	188.3	2.41	0.70	0.02	0.99	Moderately sorted	Symmetrical	Mesokurtic
7-S*	Unimodal	216.5	2.21	0.50	0.17	1.04	Well sorted	Fine skewed	Mesokurtic
FLS-1	Unimodal	2.99	8.36	1.50	0.01	0.90	Poorly sorted	Symmetrical	Platykurtic

has the highest trace element concentrations; by contrast, sample 1 has the lowest concentrations, except for Zr and Hf, which are usually enriched in zircon and in the relatively coarse-grained fraction (García et al., 1994; López et al., 2005). However, the trace element concentrations of the clay dunes are much higher than those of the fine fraction of sample 8 (Fig. 6b). The fluvial-lacustrine sediments (samples FLS-1, FLS-2) exhibit a different pattern to the other samples (Fig. 6b), with higher concentrations of Sr, Sc and Li and lower concentrations of HFSE (Th, U, Nb, Ta, Zr, Hf, Y).

The chondrite-normalized REE distribution patterns (Taylor and McLennan, 1985) are illustrated in Fig. 6c, d. All of the samples, especially the bulk samples, exhibit a similar REE distribution pattern, characterized by a steep light-REE (LREE) distribution and negative Eu anomalies. Like the trace elements (Fig. 6b), Σ REE exhibits a varying degree of enrichment in the fine fraction (Fig. 6d); for example, in samples 3 and 9, Σ REE increases significantly from 125.4 ppm and 122.2 ppm to 319.9 ppm and 330.3 ppm. By contrast, the enrichment of REE is minor or absent for samples 2 and 8, ranging from 123.2 ppm and 131.5 ppm to 179.4 ppm and 147.6 ppm, respectively. In general, the clay dune samples have higher REE concentrations due to their high silt content, whereas the sand dune samples have a lower REE concentration arising from the dilution effect of quartz mineral (Yang et al., 2007). The fluvial-lacustrine sediments (samples FLS-1, FLS-2) demonstrate a similar REE distribution pattern to the other samples (Fig. 6c, d), especially in the case of the bulk samples; nevertheless, the REE abundance are lower than those of the fine fractions, as is also the case for the trace element content. This could be the result of relative differences in heavy mineral concentration (McLennan, 1989; López et al., 2005), as shown in Table 1, sample FLS-1 has a clay content of 35.9%.

4.4. Potential sand transport

Wind roses based on monthly records for 1983–2012 from the two nearest meteorological stations (Bayan Mod and Hails), from the margins of the SHT Basin, show that the directions of the sand-transporting winds are different. At Bayan Mod, the dominant winds are from the NW (Fig. 1), driven by the winter monsoon blowing from the Siberian High Pressure, with DP and RDD of 280.8 vector units (VU) and 120.5°, respectively. At Hails, however, the sand moving winds are multidirectional and mainly from the SW and SE (Fig. 1), with DP and RDD values of 608.9 VU and 42.7°, respectively. Local topography appears to have a strong influence on the wind regime of the SHT Basin, as indicated by the ERA-Interim reanalysis wind data (Fig. 2b), resulting in a bidirectional regime with sand transport mainly from the W and WNW directions. Their proportion, accounting for the total drift potential, decreases northeastwards from 80% to 62%, but the annual sand drift potential from the WSW and NE sectors increases from 2 to 24 VU and from 5 to 15 VU, respectively. In addition, the RDD are 110° and 102° in the center and northeast margins of the SHT Basin, respectively. ERA-Interim reanalysis data potentially provide an important information source for wind field applications and they have been widely used in geomorphology and meteorology (Gao et al., 2018; Shanas and Kumar, 2014; Torralba et al., 2017), especially in areas where meteorological stations are lacking. Kaiser-Weiss et al. (2015) compared reanalysis near-surface wind data for of the recent years (2007–2010) with station observations and demonstrated a high correlations ($r > 0.9$) between data from stations and reanalysis monthly mean wind speeds across Germany. However, small-scale topographic influences can result in pronounced differences between reanalysis

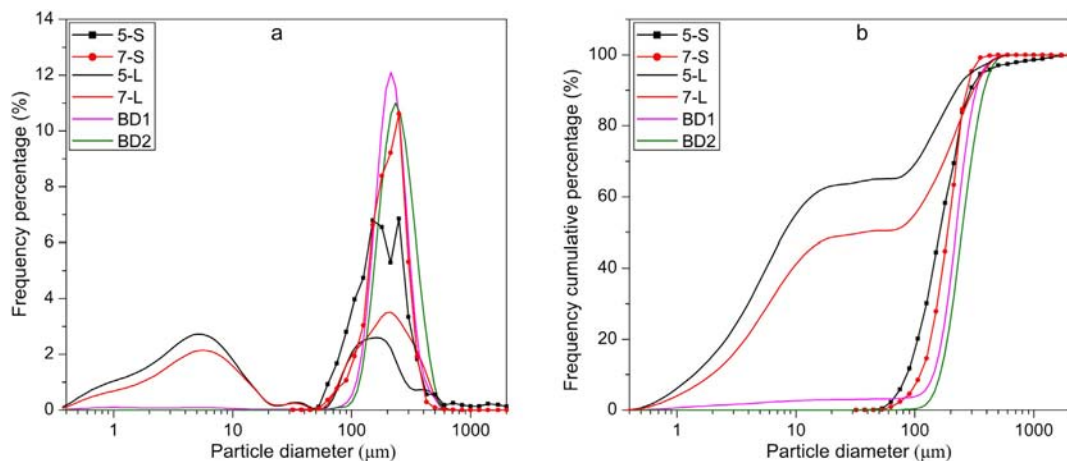


Fig. 5. Comparison of the grain-size distributions and cumulative frequency distribution curves of clay dune samples and aeolian dune sand sediments determined by standard sieving and by laser granulometry. Suffixes –S and –L represent grain size determined by standard sieving and laser granulometry, respectively.

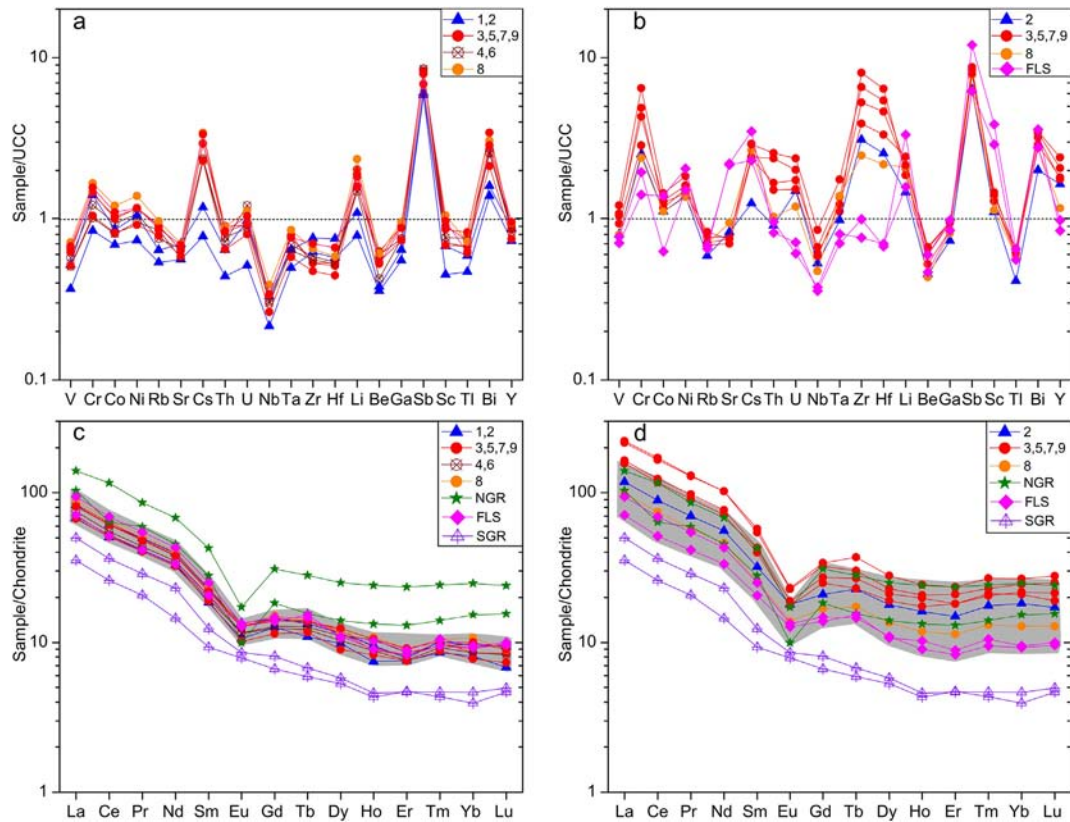


Fig. 6. Geochemical characteristics of clay dune samples and their potential sources. (a), (b) are UCC-normalized trace element patterns of bulk samples and fine fractions, respectively; (c), (d) are chondrite-normalized REE patterns of bulk samples and fine fractions, respectively. The dotted lines in (a) and (b) indicate that the elements of samples are depleted or enriched, compared to the Upper Continental Crust (UCC) (Taylor and McLennan, 1985). Above dotted line represents enrichment. The order of rare earth elements are based on atomic mass. Data of samples 1–9 are from Hu and Yang (2016). The NGR and SGR represent the granitoids from East Altay Mountains and Shalazha Mountains, respectively (data from Shi et al., 2014; Han et al., 2010).

data and station observations, due to the model height differing from the height of the actual topography (Kaiser-Weiss et al., 2015).

5. Discussion

5.1. Morphology and migration of clay dune

Morphologically, in contrast to the clay dunes in Australia, Africa and North America (Bowler, 1973; Holliday, 1997), most of those in the

study area are linear (or seif dune) and asymmetrical barchan dunes, with the lee slope steeper than the windward slope (Fig. 7c, d, g). Similar examples (longitudinal dunes of normal type) were documented in the Volga Delta by Price (1963). The differences in morphology may be caused by the diversity of local conditions such as wind regime, hydrologic conditions, and the physical nature of sediment sources. In contrast to the clay dunes forming on the margins of playas or pans with seasonal hydrological changes (Bowler, 1973; Holliday, 1997), those of area A1 are formed in areas of exposed former lake floor in the center

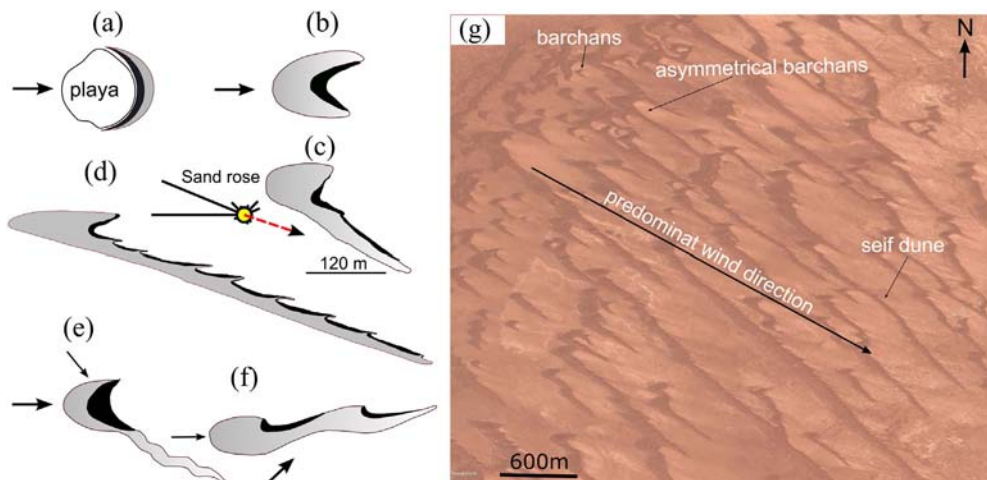


Fig. 7. (a) Clay dunes on the margin of playas (after Bowler, 1973); (b) normal barchan sand dune; (c) and (d) asymmetrical barchans and seif dunes mapped from Google Earth images; (e) and (f) conceptual model of the transition in dune shape from barchan to seif dunes proposed by Tsoar (1984) and Bagnold (1941), respectively (bold arrows represent strong winds); (g) barchans, asymmetrical barchans and seif dunes developing sequentially along the predominant wind direction (NWN-SES).

of the SHT basin. The rapid accumulation rate and high mobility associated with relatively low clay and silt contents of the dunes (Table 1) (Dare-Edwards, 1984), together with the bimodal wind regime (Fig. 2) and prolonged droughts (Yang et al., 2010), dunes with a reversed shape and steep slip face do not develop (Price, 1963; Bowler, 1973; Dare-Edwards, 1984). The clay dunes in Australia, Africa and North America, as described by Bowler (1973) and Holliday (1997), are commonly crescentic in shape, with the horns pointing towards the wind, and the windward slope is steeper than the lee side, showing a reverse orientation to the barchan sand dunes (Fig. 7a, b). The origin and morphology of this type of dune is discussed in detail in Bowler (1973).

A distinguishing feature of the clay dunes in the SHT Basin is the co-existence of different dune types (Fig. 7g). Barchans, asymmetrical barchans and linear (or seif) dunes are developed sequentially along the predominant wind direction (NWN-SES) (Fig. 7g), demonstrating in detail the transformation processes of the clay dunes. Widespread seif dunes in area A1 form by the elongation of one barchan limb during migration. The morphological transition of clay dunes indicates an asymmetric bimodal wind regime and increasing sediment supply sources (Bagnold, 1941; Tsoar, 1984; Bourke, 2010; Parteli et al., 2014). However, the transition mechanism, which is critical for interpreting dune evolution and investigating the climate regime, remains controversial (Bagnold, 1941; Tsoar, 1984; Tsoar and Parteli, 2016; Lv et al., 2016). Bagnold (1941) first proposed a conceptual model to explain transitions in dune shape from barchans to seif or linear dunes. According to this model, an asymmetrical barchan is oriented parallel to the gentle wind direction, and occasional strong winds from a secondary direction elongate the horn on the side from which the stronger wind blows (Fig. 7f); examples occur in the Namib Desert (Lancaster, 1980). Tsoar (1984) later modified this model based on the field observation in Sinai. It is argued that strong winds from the primary direction and gentle winds from the secondary direction both play a part in elongating the horn on the side opposite to the gentle winds (Fig. 7e). Field observations from Peru and Qatar support this model (Bourke, 2010). Both of these two models, together with field examples, show that the divergence angle between the strong and gentler winds are acute. However,

recent numerical simulations suggested that a bimodal wind with an obtuse divergence angle could also cause limb extension (Parteli et al., 2014; Gao et al., 2015), triggering the evolution of a seif or linear dune if the transport rate between the primary and secondary winds is suitable (Bourke, 2010; Parteli et al., 2014; Gao et al., 2015). The sand rose in Fig. 7 shows that the RDD of the bimodal wind in the SHT Basin is 110° . The dominant W winds initiate the eastward movement of the barchans ($90\text{--}100^\circ$), while secondary NNW winds lead to the south-eastward ($120\text{--}130^\circ$) elongation of the southern limb of the barchans (Fig. 8). Therefore, the seif dunes evolution in the SHT Basin tend to support Tsoar's (1984) model.

Although clay dunes have been extensively identified and studied, their migration rates have never been measured. In addition, the lateral migration of seif or linear dunes remains controversial (Hesp et al., 1989; Bristow et al., 2000; Livingstone, 2003; Tsoar et al., 2004; Rubin et al., 2008; Lucas et al., 2015). In this study, we measured the migration rates of different clay dune forms based on the historical Google Earth images, which have been proved to be effective and been widely employed to assess the migration rate of dunes (Lorenz et al., 2013; Hamdan et al., 2016). Results show that during 2003–2013 the barchans and asymmetrical barchans migrated by ~ 167 m and ~ 160 m (with rates of 16.7 m/yr and 16 m/yr) (Fig. 8a, b). This demonstrates that the migration rate does not decrease significantly during the transition in morphology from barchan to asymmetrical barchan. The asymmetrical barchans also had an oblique migration of 33 m during 2003–2013 (a rate of 3.3 m/yr). Seif and linear dunes laterally migrated and elongated (Fig. 8c, d), and the northeastward lateral migration was about 20–40 m during 2003–2013 (a rate of about 2–4 m/yr), a similar rate reported for other sites in the Qaidam Basin in north China (Hesp et al., 1989). The elongation was about 100–200 m, a rate of 16–20 m/yr. Our results support the idea that seif or linear dunes can migrate laterally, although the migration rate is very low.

5.2. Origin of the clay dunes in the Alashan Plateau Desert

Modern clay dunes are known from various regions representing a relatively wide range of climatic and environmental conditions, ranging

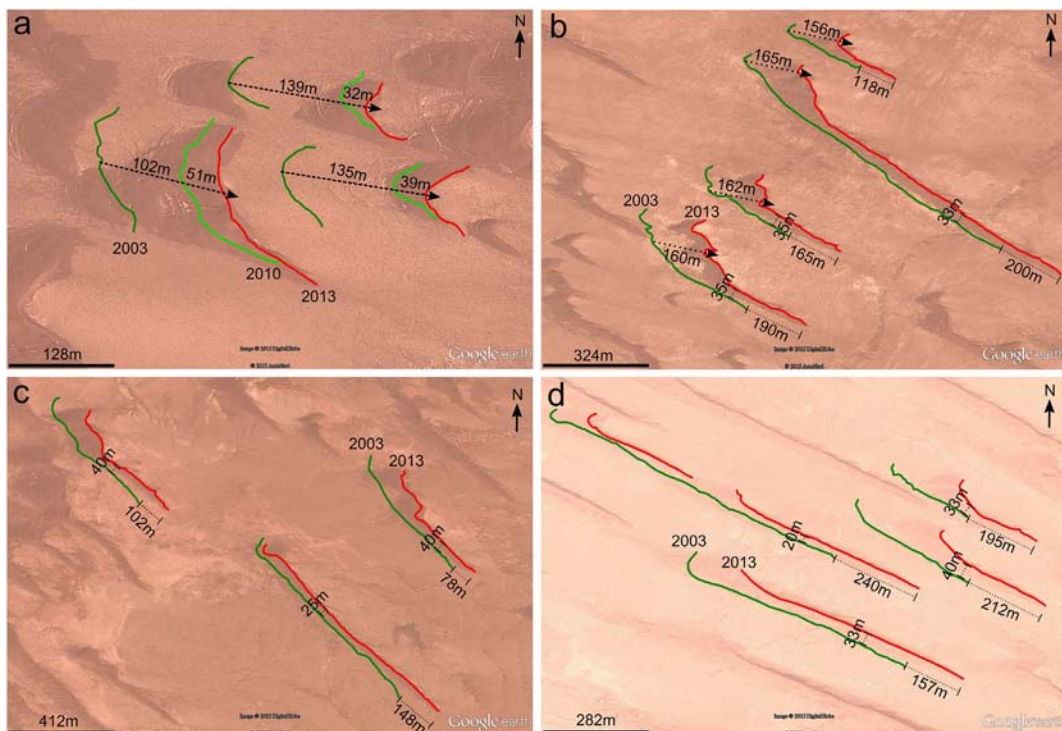


Fig. 8. Migration of the clay dunes. (a) Barchans; (b) asymmetrical barchans; (c) and (d) seif dunes. Note the lateral migration and elongation of the seif dune.

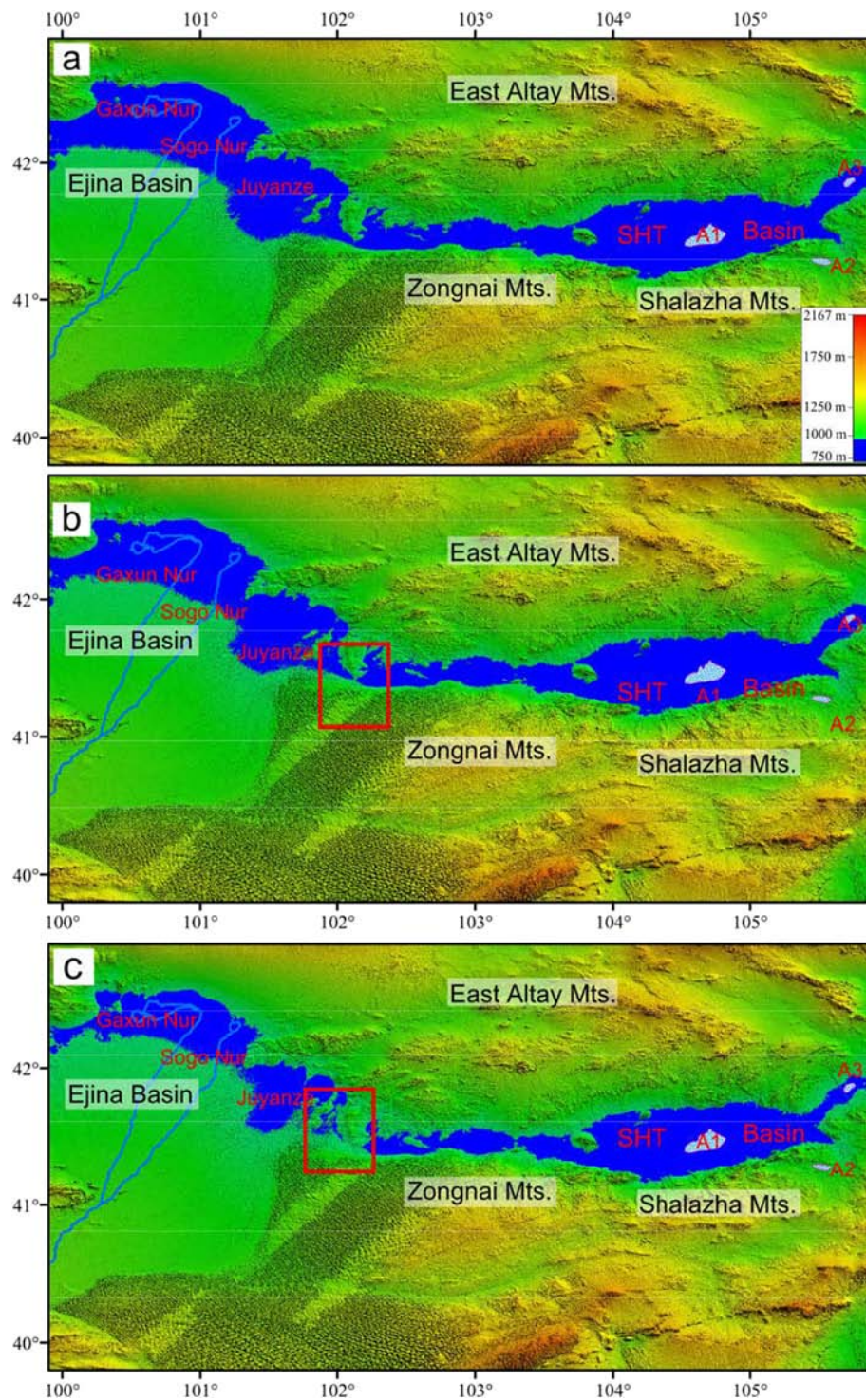


Fig. 9. DEM analysis of paleolake levels at a paleolake level at elevations of (a) 943 m, (b) 938 m and (c) 927 m under modern geomorphological conditions in Alashan Plateau. The blue shaded area represents the potential areas of the Ejina paleolake, and the red box highlights the disintegration of the integrated paleo-megalake drainage system.

from the arid and semi-arid basins of the North African deserts to the sub-humid regions of the Gulf Coast of Texas, and even the seasonally humid tropics of the west coast of Africa (Huffman and Price, 1949; Bowler, 1976; Goudie and Wells, 1995). However, in terms of their specific occurrence and distribution they are restricted to topographic depressions, such as former lake basins, playas and pans, where large amounts of fluvial-lacustrine sediments provide the source materials for their formation (Bowler, 1973; Holliday et al., 2008). Therefore, it is clear that the formation of clay dune is closely related to lake-basin evolution.

Stratigraphic evidence suggests the SHT Basin was a larger inter-montane lake during the Cretaceous (Li and Zhou, 1997). Moreover, a mega paleolake likely developed in the area during the Quaternary, as evidenced by the paleo-drainage system (Guo et al., 2000). Although detailed research on the SHT lake basin is scarce, the lake level changes of the neighboring Ejina lake basin can also provide some potential information on its evolution. Previous research on the paleo-shoreline of the Ejina Basin suggests that the lake level in Juyanze (a lake in the Ejina Basin) was as high as 940–950 m during the Mid-Late Pleistocene

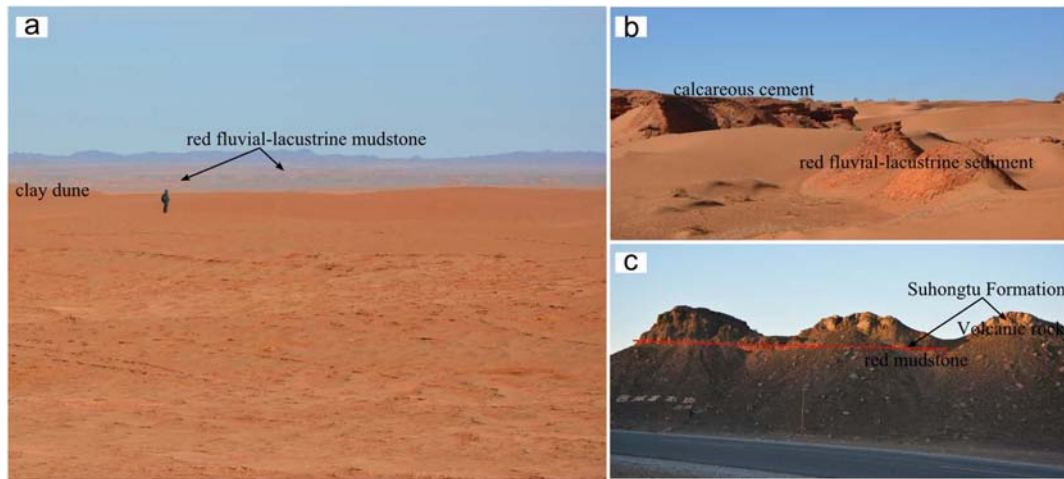


Fig. 10. Photographs illustrating the widespread Cretaceous-Tertiary and Quaternary red fluvial-lacustrine mudstone and sediments in SHT Basin.

(Wang et al., 2004; Lv et al., 2010), and as high as 926 m (Wünnemann et al., 1998, Wünnemann, 1999) and 930–932 m (Wünnemann and Hartmann, 2002) in Gaxun Nur and Sogo Nur (two lakes in Ejina Basin) during marine isotope stage 3 (MIS 3). Recent studies have shown that a megalake developed in the Ejina Basin, at a lake level of 927 m, and occupied an area of ~8000 km² during MIS 5 (Li et al., 2015, 2017), while the paleolake fluctuated frequently within the range of 912–927 m during the Holocene (Jin et al., 2015). Using a digital elevation model (DEM) for the present day topography we plotted the potential areas of the Ejina paleolake level at elevations of 943 m, 938 m and 927 m, respectively (Fig. 9). The results show that the SHT Basin would have been filled with water, since the connecting channel would have been reactivated when the lake level of the Ejina Basin reached 943 m at 142 ± 9 ka (Fig. 9a) (Lv et al., 2010). By contrast,

when the lake level dropped to 938 m, the previously interconnected paleolake drainage system started to separate (Fig. 9b). It can be inferred that the SHT paleolake would have shrank rapidly due to the decrease of the water supply, although detailed process are unknown at present.

By contrast, compound clay dunes consist of alternating clay pellet and quartz sand facies, which represent two distinct hydrological environments: a high water-level status with quartz sand facies and a low water-level with clay pellet facies (Bowler, 1973, 1986). The absence of quartz sand facies and limited areal extent of the modern active clay dunes in SHT Basin suggests that clay dunes developed after the lake basin dried up (Bowler, 1973, 1986). Therefore, the landscape of modern clay dunes in SHT Basin could not have predated MIS 5. Notably, specific climatic, hydrological and sedimentary environments are



Fig. 11. The Landsat 8 OLI-TRIS images (data set is provided by Geospatial Data Cloud site, Computer Network Information Center, Chinese Academy of Sciences, <http://www.gscloud.cn>) showing the three areas of clay dune development. Note the occurrences of red mudstone and terminal alluvial fans.

Table 3
Geochemical data for different samples showing evaporates origin of the clay dunes.

Sample	CaO (%)	MgO (%)	Li (ppm)	Be (ppm)	Ga (ppm)	Rb (ppm)	Sr (ppm)	Cs (ppm)	Sc (ppm)	Bi (ppm)
1	1.94	0.82	15.7	1.07	9.36	60.1	196	2.88	4.97	0.176
2	2.74	1.85	21.7	1.14	10.9	71.5	244	4.37	7.46	0.203
3	3.23	2.12	36.5	1.73	15.3	101	224	10.8	9.92	0.343
4	4.25	1.77	31.3	1.79	12.8	84.4	229	8.72	8.43	0.323
5	2.94	2.09	40.4	1.88	15.2	102	223	10.9	9.48	0.434
6	2.39	1.45	29.7	1.28	12.7	95.2	199	8.54	7.81	0.326
7	2.37	1.65	31.8	1.62	12.5	87.9	205	8.49	7.51	0.27
8	3.15	2.54	46.9	1.82	16.2	108	245	12.7	11.5	0.388
9	3.29	2.29	37.9	1.58	14.9	97.4	241	12.4	10.6	0.363
FLS-1	8.82	9.19	66.60	1.40	14.40	73.00	774.00	12.90	14.30	0.35
FLS-2	2.52	1.82	31.50	1.79	16.60	76.20	757.00	8.51	10.70	0.46

required for the development of clay dunes (Bowler, 1973; Holliday, 1997; Lawson and Thomas, 2002). Generally, the formation of a dune field is dependent on sediment availability and aeolian transport capacity (Thomas, 2011), and thus a dry-cold and windy climate could provide more source materials and enhance sediment transport capacity (Kocurek and Lancaster, 1999; Lancaster et al., 2002; Pye and Tsoar, 2008; Thomas, 2011). Although the cold, dry and windy climate which occurred in the study region during the last glacial maximum (LGM) (Wünnemann et al., 2007; Gao et al., 2006) was conducive to the formation of clay dunes (Bowler, 1973; Rich, 2013), the subsequent more humid and rainy climate during the early Holocene and Holocene Optimum (HO) (Yang et al., 2010, 2011) would have contributed to lake or wetland development in SHT Basin. More humid and rainy climate was also conducive to development of rivers or channels around the SHT Basin, and the mount of water inputs into the paleo-lakes will increase greatly. Although its possible extent may be limited, it could inhibit the development of clay dunes, and even inundated and flooded the pre-existing clay dunes. By contrast, the repeated episodes of intense aridity in the late Holocene (Yang et al., 2003, 2011) could favor the accumulation of clay dunes. Many studies demonstrate that aeolian activities have significantly enhanced in the desert belt of north China since 4 ka (Yang et al., 2010; Fan et al., 2010; Lu et al., 2005; Li and Yang, 2016). Therefore, we suggest that the landscape of modern clay dunes in the SHT Basin could be formed since late Holocene. However, the precise age of the onset of modern clay dune formation in SHT Basin requires more detailed chronostratigraphic studies in the future.

5.3. Sediment source of the clay dunes

Clay dunes are mainly composed of clay and silt and therefore source materials with a high content of material within these grades are needed for their formation (Bowler, 1973, 1986). Thus, we consider that the potential source materials are likely derived from local fluvial-lacustrine sediments which were deflated from the SHT Basin and accumulated as sand-sized aggregates in the clay dunes. Cretaceous-Tertiary and Quaternary red fluvial-lacustrine mudstone (Fig. 10) is widespread in the SHT Basin and could have contributed silts and clays to the basin system via the drainage network. As shown in Fig. 10, red fluvial-lacustrine mudstone, which could supply clays and silts to the central basin via stream or runoff and/or deflation (Holliday, 1997), occurs in the west and northwest sectors of the clay dune field. Moreover, the Landsat 8 OLI-TRIS images (Fig. 11) also show that all the three clay dune fields situate in the places where red mudstone outcrops and terminal alluvial fans occur (Fig. 11). Thus, we suggest that the clay and silt materials eroded from the mudstone were transported by runoff and deposited in the basin; clay pellets were then produced by the deflation of these alluvial deposits to form the clay dunes (Dare-Edwards, 1984). This linkage is supported by the observation that the grain-size distributions of both the red fluvial-lacustrine sediments (FLS-2) and the clay dune sediments exhibit a main mode at around 4–6 μm (Fig. 4),

confirming that the local Cretaceous-Tertiary and Quaternary red fluvial-lacustrine mudstone is the main source of the clay dunes.

Our interpretation of the sediment source of the clay dunes is also supported by geochemical evidence. Geochemical fingerprinting has great potential for tracing the source of sediments (Taylor and McLennan, 1985; McLennan, 1989; Yang et al., 2007a; Muhs et al., 2013; Lancaster et al., 2015; Hu and Yang, 2016), especially trace elements and REE, because they are less subject to fractionation during weathering, transport and sedimentation (McLennan, 1989; Murray, 1994; López et al., 2005). Compared to the sand dune sample (sample 1), the samples from the clay dunes, as well as the fluvial-lacustrine samples FLS-1 and FLS-2, are finer-grained and relatively enriched in elements indicative of an evaporative origin, such as Mg, Ca and the trace elements Sr and Li (Table 3), which are likely to be incorporated as substitute elements in evaporate minerals (Schreiber and Tabakh, 2000; Telfer and Thomas, 2006). The higher abundances of Ga, Sc, Bi, Rb and Cs (Table 3) also indicate a greater contribution of materials of lacustrine and evaporative origin (Shi, 1987; Sun et al., 1992; Rollinson, 1993). The absence of enrichment of Na may be the result of its being more easily leached soon after deposition (Bowler, 1973). In addition, the REE content of the clay dune sediments has a similar distribution to that of the fluvial-lacustrine samples (Figs. 6c, d), implying a close relationship between the two. However, the sand dune samples (samples 1 and 2) also show similar REE patterns to those of the clay dunes. This may be explained by: 1) the clay dunes in the study area have a higher sand concentration, 2) the clay dunes and sand dunes have an identical ultimate source. Compared to clay dunes in Australia where the clay and silt content reaches 80–90% (Bowler, 1973, 1983), the clay and silt contents of clay dunes in the study area are much smaller, within the range of 30–71%. Geochemical evidence suggests that the sediments of the clay dunes and sand dunes are all derived from the weathered and denuded products of Permian granitoid source rocks (Hu and Yang, 2016). Comparing to the rock of granitoids from the East Altay Mountains and Shalazha Mountains (Han et al., 2010; Shi et al., 2014), clay dunes, sand dunes and fluvial-lacustrine samples have more similar REE patterns to the granitoids from the East Altay Mountains (Fig. 6c, d), implying the source sediments should originate from the East Altay Mountains, rather than the Shalazha Mountains.

6. Conclusions

Three isolated clay dune fields have been identified in the SHT Basin of Alashan Plateau in north China, based on field investigations and analysis of satellite images. The clay dunes are all developed in lowland and occupy areas ranging from ~30 to ~254 km². Several types of clay dune co-exist in the area, including barchans, hooked barchans, asymmetrical barchans and linear or seif dunes. Their morphology distinguishes them from most of the well-studied clay dunes in Australia, Africa and America, and the asymmetrical bimodal wind regime, prolonged drought and relatively low clay and silt content are likely responsible for the differences. Our results support Tsoar's (1984) model

of dune shape transition from barchans to seif or linear dunes. Linear (seif) dunes laterally migrated and elongated at a rate of about 2–4 m/yr and 16–20 m/yr, respectively. Based on knowledge of the evolution of the SHT paleo-lake basin and regional climate change, we argue that the landscape of modern clay dunes in SHT Basin could not predate MIS 5, and probably formed since the late Holocene. The grain-size composition of clay dune samples are characterized by a high percentage of silt and clay, 29.56% to 65.10%. The silt and clay were deflated, transported and accumulated as sand-sized aggregates of clay pellets. The trace elements and REE patterns of the clay dune samples are different to those of the sand dune samples, with an elevated concentration of elements of evaporative origin (e.g., Sr, Li, Rb, Cs). Comparison of the trace element and REE patterns of the clay dune samples with those of red fluvial-lacustrine sediments and rocks in their potential source areas, together with particle size and geomorphological analysis, leads us to conclude that the source sediments of the clay dunes are mainly derived from local Cretaceous-Tertiary and Quaternary red fluvial-lacustrine mudstone and sediments, and that the ultimate source is the granitoids of the East Altay Mountains.

Acknowledgements

This research was supported by the National Natural Science Foundation of China (Grant nos. 41430532, 41501224 and 41801009) and the Science and Technology Project of the Education Department of Jiangxi Province, China (No. GJJ180858). We thank Prof. Deguo Zhang from Zhejiang University for helpful discussions of dune morphology. Sincere thanks are extended to Editor Prof. Martin Stokes and two anonymous reviewers for their constructive comments on the earlier draft of this paper.

References

- Bagnold, R.A., 1941. *The Physics of Blown Sand and Desert Dunes*. Chapman and Hall, London.
- Bernat Rebollal, M., Pérez-González, A., 2008. Inland aeolian deposits of the Iberian Peninsula: Sand dunes and clay dunes of the Duero Basin and the Manchega Plain. *Geomorphology* 102, 207–220.
- BGMIRM (Bureau of Geology and Mineral Resources of Inner Mongolia), 1991. *Regional Geology of Nei Mongol (Inner Mongolia) Autonomous Region*. Geological Publishing House, Beijing (in Chinese with English summary).
- Blott, S.J., Pye, K., 2001. GRADISTAT: a grain size distribution and statistics package for the analysis of unconsolidated sediments. *Earth Surf. Process. Landf.* 26, 1237–1248.
- Bourke, M.C., 2010. Barchan dune asymmetry: Observations from Mars and Earth. *Icarus* 205, 183–197.
- Bowen, M.W., Johnson, W.C., 2012. Late Quaternary environmental reconstructions of playa-lunette system evolution on the central High Plains of Kansas, United States. *Geol. Soc. Am. Bull.* 124, 146–161.
- Bowler, J.M., 1973. Clay Dunes: their Occurrence, Formation and Environmental significance. *Earth Sci. Rev.* 9, 315–338.
- Bowler, J.M., 1976. Aridity in Australia: Age, Origins and Expression in Aeolian Landforms and Sediments. *Earth Sci. Rev.* 12, 279–310.
- Bowler, J.M., 1983. Lunettes as indices of hydrologic change: a review of Australian evidence. *Proc. Roy. Soc. Victoria* 95, 147–168.
- Bowler, J.M., 1986. Spatial variability and hydrologic evolution of Australian lake basins: analogue for Pleistocene hydrologic change and evaporite formation. *Palaeogeogr. Palaeoclimatol. Palaeoecol.* 54, 21–41.
- Bristow, C.S., Bailey, S.D., Lancaster, N., 2000. The sedimentary structure of linear sand dunes. *Nature* 406, 56–59.
- Chen, X.Y., 1995. Geomorphology, stratigraphy and thermoluminescence dating of the lunette dune at Lake Victoria, western New South Wales. *Palaeogeogr. Palaeoclimatol. Palaeoecol.* 13, 69–86.
- Coffey, G.N., 1909. Clay Dunes. *J. Geol.* 17, 754–755.
- Dangavs, N.V., 1979. Presencia de dunas de argilla fosiles en la Pampa Deprimada. *Revista Asociación Geologica Argentina* 34, 31–35.
- Dare-Edwards, A.J., 1984. Aeolian clay deposits of South-Eastern Australia: parna or loessic clay? *Trans. Inst. Br. Geogr.* 9, 337–344.
- Edwin, S., Hills, D.S., 1940. The lunette, a new land form of aeolian origin. *Aust. Geogr.* 7, 15–21.
- Fan, Y., Chen, F., Fan, T., Zhao, H., Yang, L., 2010. Sedimentary documents and Optically Stimulated Luminescence (OSL) dating for formation of the present landform of the northern Ulan Buh Desert, northern China. *Sci. China Earth Sci.* 53, 1675–1682.
- Fitzsimmons, K.E., Bowler, J.M., Rhodes, E.J., Magee, J.M., 2007. Relationships between desert dunes during the late Quaternary in the Lake Frome region, Strzelecki Desert, Australia. *J. Quat. Sci.* 22, 549–558.
- Folk, R.L., Ward, W.C., 1957. Brazos River bar: a study in the significance of grain size parameters. *J. Sediment. Res.* 27, 3–26.
- Fryberger, S.G., Dean, G., 1979. Dune forms and wind regime. In: McKee, E. (Ed.), *A Study of Global Sand Seas*. United States Geological Survey Professional Paper. vol. 1052, pp. 137–169 Washington.
- Gao, Q., Tao, Z., Li, B., Jin, H., Zou, X., Zhang, Y., Dong, G., 2006. Palaeomonsoon variability in the southern fringe of the Badain Jaran Desert, China, since 130 ka BP. *Earth Surf. Process. Landf.* 31, 265–283.
- Gao, X., Narteau, C., Rozier, O., du Pont, S.C., 2015. Phase diagrams of dune shape and orientation depending on sand availability. *Sci. Rep.* 5, 14677.
- Gao, X., Gadal, C., Rozier, O., Narteau, C., 2018. Morphodynamics of barchan and dome dunes under variable wind regimes. *Geology* 46, 743–746.
- Garcia, D., Fontelles, M., Moutte, J., 1994. Sedimentary fractionations between Al, Ti, and Zr and the genesis of strongly peraluminous granites. *J. Geol.* 102, 411–422.
- Goudie, A.S., Wells, G.L., 1995. The nature, distribution and formation of pans in arid zones. *Earth Sci. Rev.* 38, 1–69.
- Guo, H., Liu, H., Wang, X., Shao, Y., Sun, Y., 2000. Subsurface old drainage detection and paleoenvironment analysis using spaceborne radar images in Alashan Plateau. *Sci. China Ser. D Earth Sci.* 43, 439–448.
- Hamdan, M.A., Refaat, A.A., Abdel Wahed, M., 2016. Morphologic characteristics and migration rate assessment of barchan dunes in the Southeastern Western Desert of Egypt. *Geomorphology* 257, 57–74.
- Han, B.F., Zhang, C., Zhao, L., Ren, R., Xu, Z., Chen, J.F., Zhang, L., Zhou, Y.Z., Song, B., 2010. A preliminary study of granitoids in western Inner Mongolia. *Acta Petrol. Mineral.* 29, 741–749 (in Chinese with English abstract).
- Hesp, P.A., Smyth, T.A.G., 2019. *Anchored Dunes*. In: Livingstone, I., Warren, A. (Eds.), *Aeolian Geomorphology: A New Introduction*. John Wiley & Sons Ltd, New Jersey, pp. 157–178.
- Hesp, P.A., Hyde, R., Hesp, V., Qian, Z., 1989. Longitudinal dunes can move sideways. *Earth Surf. Process. Landf.* 14, 447–451.
- Holliday, V.T., 1997. Origin and Evolution of Lunettes on the High Plains of Texas and New Mexico. *Quat. Res.* 47, 54–69.
- Holliday, V.T., Mayer, J.H., Fredlund, G.G., 2008. Late Quaternary sedimentology and geochronology of small playas on the Southern High Plains, Texas and New Mexico, U.S.A. *Quat. Res.* 70, 11–25.
- Hu, F., Yang, X., 2016. Geochemical and geomorphological evidence for the provenance of aeolian deposits in the Badain Jaran Desert, northwestern China. *Quat. Sci. Rev.* 131, 179–192.
- Huffman, G.G., Price, W.A., 1949. Clay dune formation near Corpus Christi, Texas. *J. Sediment. Res.* 19, 118–127.
- Jin, M., Li, G., Li, F., Duan, Y., Wen, L., Wei, H., Yang, L., Fan, Y., Chen, F., 2015. Holocene shorelines and lake evolution in Juyanze Basin, southern Mongolian Plateau, revealed by luminescence dating. *The Holocene* (12), 1898–1911.
- Kaiser-Weiss, A.K., Kaspar, F., Heene, V., Borsche, M., Tan, D.G.H., Poli, P., Obregon, A., Gregow, H., 2015. Comparison of regional and global reanalysis near-surface winds with station observations over Germany. *Adv. Sci. Res.* 12, 187–198.
- Killigrew, L.P., Gilkes, R.J., 1974. Development of playa lakes in South Western Australia. *Nature* 247, 454–455.
- Kocurek, G., Lancaster, N., 1999. Aeolian system sediment state: theory and Mojave Desert Kelso dune field example. *Sedimentology* 46, 505–515.
- Lancaster, N., 1978. The Pans of the Southern Kalahari, Botswana. *Geogr. J.* 144, 81–98.
- Lancaster, N., 1980. The formation of seif dunes from barchans – supporting evidence for Bagnold's model from the Namib Desert. *Z. Geomorph. N. F.* 24, 160–167.
- Lancaster, N., 1986. Pans in the southwestern Kalahari: a preliminary report. *Palaeoecol. Afr.* 17, 59–67.
- Lancaster, N., 1995. *Geomorphology of Desert Dunes*. Routledge, London, p. 73.
- Lancaster, N., Kocurek, G., Singhvi, A., Pandey, V., Deynoux, M., Ghienne, J., Lô, K., 2002. Late Pleistocene and Holocene dune activity and wind regimes in the western Sahara Desert of Mauritania. *Geology* 30, 991–994.
- Lancaster, N., Baker, S., Bacon, S., McCarley-Holder, G., 2015. Owens Lake dune fields: Composition, sources of sand, and transport pathways. *Catena* 134, 41–49.
- Lawson, M.P., Thomas, D.S.G., 2002. Late Quaternary lunette dune sedimentation in the southwestern Kalahari Desert, South Africa: luminescence based chronologies of aeolian activity. *Quat. Sci. Rev.* 21, 825–836.
- Lees, B.G., Cook, P.G., 1991. A conceptual model of lake barrier and compound lunette formation. *Palaeogeogr. Palaeoclimatol. Palaeoecol.* 84, 271–284.
- Li, H., Yang, X., 2016. Spatial and temporal patterns of aeolian activities in the desert belt of northern China revealed by dune chronologies. *Quat. Int.* 40, 58–68.
- Li, H., Zhou, L., 1997. Sedimentary facies and tectonic setting of the cretaceous in the Suhongtu-Yingen Basin. *Sci. Geol. Sin.* 32, 387–396 (in Chinese with English abstract).
- Li, G., Jin, M., Duan, Y., Madsen, D.B., Li, F., Yang, L., Wei, H., Chen, F., 2015. Quartz and K-feldspar luminescence dating of a Marine Isotope Stage 5 megalake in the Juyanze Basin, Central Gobi Desert, China. *Palaeogeogr. Palaeoclimatol. Palaeoecol.* 440, 96–109.
- Li, G., Li, F., Jin, M., She, L., Duan, Y., Madsen, D., Wang, L., 2017. Late Quaternary lake evolution in the Gaxun Nur basin, central Gobi Desert, China, based on quartz OSL and K-feldspar pIRIR dating of paleoshorelines. *J. Quat. Sci.* 32, 347–361.
- Livingstone, I., 2003. A twenty-one-year record of surface change on a Namib linear dune. *Earth Surf. Process. Landf.* 28, 1025–1031.
- López, J.M.G., Bauluz, B., Fernández-Nieto, C., Oliete, A.Y., 2005. Factors controlling the trace-element distribution in fine-grained rocks: the Albian kaolinite-rich deposits of the Oliete Basin (NE Spain). *Chem. Geol.* 214, 1–19.
- Lorenz, R.D., Gamsi, N., Radebaugh, J., Barnes, J.W., Ori, G.G., 2013. Dunes on planet Tatooine: Observation of barchan migration at the Star Wars film set in Tunisia. *Geomorphology* 201, 264–271.

- Lu, H., Miao, X., Zhou, Y., Mason, J., Swinehart, J., Zhang, J., Zhou, L., Yi, S., 2005. Late Quaternary aeolian activity in the Mu Us and Otindag dune fields (North China) and lagged response to insolation forcing. *Geophys. Res. Lett.* 32, L21716.
- Lucas, A., Narteau, C., Rodriguez, S., Rozier, O., Callot, Y., Garcia, A., Courrech Du Pont, S., 2015. Sediment flux from the morphodynamics of elongating linear dunes. *Geology* 43, 1027–1030.
- Lv, Y., Gu, Z., Aldahan, A., Zhang, H., Possnert, G., Lei, G., 2010. ^{10}Be in quartz gravel from the Gobi Desert and evolutionary history of alluvial sedimentation in the Ejina Basin, Inner Mongolia, China. *Chin. Sci. Bull.* 55, 3802–3809.
- Lv, P., Dong, Z., Narteau, C., Rozier, O., 2016. Morphodynamic mechanisms for the formation of asymmetric barchans: improvement of the bagnold and tsoar models. *Environ. Earth Sci.* 75, 1–9.
- Marker, M.E., Holmes, P.J., 1995. Lunette dunes in the northeast Cape, South Africa, as geomorphic indicators of palaeoenvironmental change. *Catena* 24, 259–273.
- McKee, E.D., 1979. A study of global sand seas. United States Geological Survey Professional Paper, p. 1052 (Washington).
- McLennan, S.M., 1989. Rare earth elements in sedimentary rocks: influence of provenance and sedimentary processes. *Rev. Mineral. Geochem.* 21, 169–200.
- Muhs, D.R., Roskin, J., Tsoar, H., Skipp, G., Budahn, J.R., Sneh, A., Porat, N., Stanley, J., Katra, I., Blumberg, D.G., 2013. Origin of the Sinai–Negev erg, Egypt and Israel: mineralogical and geochemical evidence for the importance of the Nile and sea level history. *Quat. Sci. Rev.* 69, 28–48.
- Munroe, J.S., Gorin, A.L., Stone, N.N., Amidon, W.H., 2017. Properties, age, and significance of dunes near snow water lake, Elko County, Nevada. *Quat. Res.* 87, 24–36.
- Murray, R.W., 1994. Chemical criteria to identify the depositional environment of chert: general principles and applications. *Sediment. Geol.* 90, 213–232.
- Parteli, E.J.R., Durán, O., Bourke, M.C., Tsoar, H., Pöschel, T., Herrmann, H., 2014. Origins of barchan dune asymmetry: Insights from numerical simulations. *Aeolian Res.* 12, 121–133.
- Price, W.A., 1963. Physicochemical and environmental factors in clay dune genesis. *J. Sediment. Petrol.* 33, 766–778.
- Pye, K., Tsoar, H., 2008. *Aeolian Sand and Sand Dunes*. Springer, Berlin Heidelberg.
- Rich, J., 2013. A 250,000-year record of lunette dune accumulation on the Southern High Plains, USA and implications for past climates. *Quat. Sci. Rev.* 62, 1–20.
- Rollinson, H.R., 1993. *Using geochemical data: evaluation, presentation, interpretation*. Routledge, New York.
- Rubin, D.M., Hesp, P.A., 2009. Multiple origins of linear dunes on Earth and Titan. *Nat. Geosci.* 2, 653–658.
- Rubin, D.M., Tsoar, H., Blumberg, D.G., 2008. A second look at western Sinai seif dunes and their lateral migration. *Geomorphology* 93, 335–342.
- Sabin, T.J., Holliday, V.T., 1995. Playas and Lunettes on the Southern High Plains: Morphometric and Spatial Relationships. *Ann. Assoc. Am. Geogr.* 85, 286–305.
- Schreiber, B.C., Tabakh, M.E., 2000. Deposition and early alteration of evaporites. *Sedimentology* 47, 215–238.
- Shanas, P.R., Sanil Kumar, V., 2014. Coastal processes and longshore sediment transport along Kundapura coast, central west coast of India. *Geomorphology* 214, 436–451.
- Shi, Y., 1987. Characteristics of salt lake and salt's forming regions in Inner Mongolia. *J. Inner Mongolia Normal Univ. (Natural Science Edition)* 15, 43–51 (in Chinese with English abstract).
- Shi, X., Wang, T., Zhang, L., Castro, A., Xiao, X., Tong, Y., Zhang, J., Guo, L., Yang, Q., 2014. Timing, petrogenesis and tectonic setting of the late Paleozoic gabbro–granodiorite–granite intrusions in the Shalazhashan of northern Alashan: Constraints on the southernmost boundary of the Central Asian Orogenic Belt. *Lithos* 208, 158–177.
- Sun, Z., Cao, C., Liang, X., Xu, K., 1992. On the facies differentiation indicator–Boron and Gallium content. *Acta Pet. Sin.* 13, 42–46 (in Chinese with English abstract).
- Sun, Y.B., Tada, R.J., Chen, J.C., Liu, Q.S., Toyoda, S., Tani, A., Ji, J.F., Isozaki, Y., 2008. Tracing the provenance of fine-grained dust deposited on the central Chinese Loess Plateau. *Geophys. Res. Lett.* 35, L01804.
- Szynkiewicz, A., Ewing, R.C., Moore, C.H., Glamoclija, M., Bustos, D., Pratt, L.M., 2010. Origin of terrestrial gypsum dunes—Implications for Martian gypsum-rich dunes of Olympia Undae. *Geomorphology* 121, 69–83.
- Taylor, S.R., McLennan, S.M., 1985. *The Continental Crust: Its Composition and Evolution*. Blackwell, Oxford.
- Telfer, M.W., Thomas, D.S.G., 2006. Complex Holocene lunette dune development, South Africa: Implications for paleoclimate and models of pan development in arid regions. *Geology* 34, 853.
- Thomas, D.S.G., 2011. *Arid zone Geomorphology: Process, Form and Change in Drylands*. John Wiley & Sons, Ltd, pp. 1–624.
- Thomas, D.S., Burrough, S.L., 2012. Interpreting geo-proxies of late Quaternary climate change in African drylands: Implications for understanding environmental change and early human behaviour. *Quat. Int.* 253, 5–17.
- Thomas, D.S.G., Nash, D.J., Shaw, P.A., Van der Post, C., 1993. Present Day Lunette Sediment Cycling at Witpan in the Arid Southwestern Kalahari Desert. *Catena* 20, 515–527.
- Torralba, V., Doblasreyes, F.J., Gonzalezreviriego, N., 2017. Uncertainty in recent near-surface wind speed trends: a global reanalysis intercomparison. *Environ. Res. Lett.* 12, 114019.
- Tsoar, H., 1984. The formation of seif dunes from barchans – a discussion. *Z. Geomorph. N.F.* 28, 99–103.
- Tsoar, H., 1978. The dynamics of longitudinal dunes. Final technical report. European Research Office, US Army, London.
- Tsoar, H., Parteli, E.J.R., 2016. Bidirectional winds, barchan dune asymmetry and formation of seif dunes from barchans: a discussion. *Environ. Earth Sci.* 75, 1237.
- Tsoar, H., Blumberg, D.G., Stoler, Y., 2004. Elongation and migration of sand dunes. *Geomorphology* 57, 293–302.
- Wang, X., Guo, H., Chang, Y., Zha, L., 2004. On paleodrainage evolution in mid-late Epileistocene based on radar remote sensing in northeastern Ejin Banner, Inner Mongolia. *J. Geogr. Sci.* 14, 235–241.
- Williams, M., 2014. *Climate Change in Deserts: Past, Present and Future*. Cambridge University Press, Cambridge, pp. 1–629.
- Wu, T., He, Q., 1993. Tectonic units and their fundamental characteristics on the northern margin of the Alashan block. *Acta Geol. Sin.* 67, 97–108 (in Chinese with English abstract).
- Wünnemann, B., 1999. Untersuchungen zur Palaeohydrographie der Endseen in der Badain Jaran- und Tengger Wüste, Innere Mongolei, Nordwest-China. Habilitation thesis, Freie Universität Berlin. Nur Basin, Inner Mongolia, China. *Z. Geomorph. N.F.* 126, 147–168.
- Wünnemann, B., Hartmann, K., 2002. Morphodynamics and Paleohydrography of the Gaxun Nur Basin, Inner Mongolia, China. *Z. Geomorph. N.F.* 126, 147–168.
- Wünnemann, B., Pachur, H.J., Li, J., Zhang, H., 1998. The chronology of Pleistocene and Holocene lake level fluctuations at Gaxun Nur/Sogo Nur and Baijian Hu in Inner Mongolia, China. *Petermanns Geogr. Mitt.* 142, 191–206.
- Wünnemann, B., Hartmann, K., Altmann, N., Hambach, U., Pachur, H., Zhang, H., 2007. Inter-glacial and glacial fingerprints from lake deposits in the Gobi Desert, NW China. *Dev. Quat. Sci.* 7, 323–347.
- Yang, X., 1991. Geomorphologische Untersuchungen in Trockenraumen NW-Chinas unter besonderer Berücksichtigung von Badanjilin und Takelamagan. *Göttinger Geogr. Abh.* 96, 1–124.
- Yang, X., Liu, T., Xiao, H., 2003. Evolution of megadunes and lakes in the Badain Jaran Desert, Inner Mongolia, China during the last 31,000 years. *Quat. Int.* 104, 99–112.
- Yang, X., Liu, Y., Li, C., Song, Y., Zhu, H., Jin, X., 2007. Rare earth elements of aeolian deposits in Northern China and their implications for determining the provenance of dust storms in Beijing. *Geomorphology* 87, 365–377.
- Yang, X., Zhu, B., White, P.D., 2007a. Provenance of aeolian sediment in the Taklamakan Desert of western China, inferred from REE and major-elemental data. *Quat. Int.* 175, 71–85.
- Yang, X., Ma, N., Dong, J., Zhu, B., Xu, B., Ma, Z., Liu, J., 2010. Recharge to the inter-dune lakes and Holocene climatic changes in the Badain Jaran Desert, western China. *Quat. Res.* 73, 10–19.
- Yang, X., Scuderi, L., Paillou, P., Liu, Z., Li, H., Ren, X., 2011. Quaternary environmental changes in the drylands of China—a critical review. *Quat. Sci. Rev.* 30, 3219–3233.
- Yang, X., Wang, X., Liu, Z., Li, H., Ren, X., Zhang, D., Ma, Z., Rioual, P., Jin, X., Scuderi, L., 2013. Initiation and variation of the dune fields in semi-arid China—with a special reference to the Hunshandake Sandy Land, Inner Mongolia. *Quat. Sci. Rev.* 79, 369–380.
- Yang, X., Scuderi, L.A., Wang, X., Scuderi, L.J., Zhang, D., Li, H., Forman, S., Xu, Q., Wang, R., Huang, W., Yang, S., 2015. Groundwater sapping as the cause of irreversible desertification of Hunshandake Sandy Lands, Inner Mongolia, northern China. *Proc. Natl. Acad. Sci.* 112, 702–706.